NANO LETTERS
Letter
Cite This: Nano Lett. 2018, 18, 1896−1902
pubs.acs.org/NanoLett

Strong Localization of Surface Plasmon Polaritons with Engineered Disorder

Wen-Bo Shi,[†] Lian-Zi Liu,[†] Ruwen Peng,*[,†] Di-Hu Xu,[†] Kun Zhang,[†] Hao Jing,[†] Ren-Hao Fan,[†] Xian-Rong Huang,*[,‡] Qian-Jin Wang,[†] and Mu Wang*[,†]

[†]National Laboratory of Solid State Microstructures, School of Physics, and Collaborative Innovation Center of Advanced Microstructures, Nanjing University, Nanjing 210093, China

[‡]Advanced Photon Source, Argonne National Laboratory, Argonne, Illinois 60439, United States

Supporting Information

ABSTRACT: In this work, we experimentally demonstrate for the first time strong localization of surface plasmon polaritons (SPPs) at visible regime in metallic nanogratings with short-range correlated disorder. By increasing the degree of disorder, the confinement of SPPs is significantly enhanced, and the effective SPP propagation length dramatically shrinks. Strong localization of SPPs eventually emerges at visible regime, which is verified by the exponentially decayed fields and the vanishing autocorrelation function of the SPPs. Physically, the short-range correlated disorder induces strong interference among multiple scattered SPPs and provides an adequate fluctuation to effective permittivity, which leads to the localization effect. Our study demonstrates a unique opportunity for disorder engineering to manipulate light on nanoscale and may achieve various applications in random nanolasing, solar energy, and strong light-matter interactions.

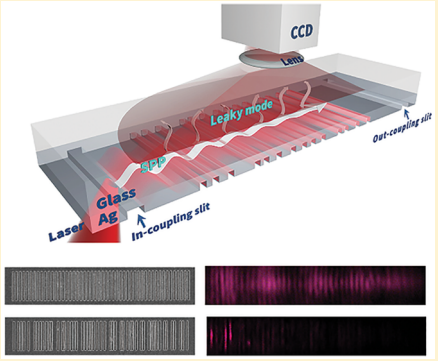

KEYWORDS: *Strong localization of surface plasmon polaritons, Short-range correlated disorder, Anderson localization, Random nanolasing*

The localization of waves in disordered systems is an important effect in condensed matter physics, which was initially investigated by Anderson in 1958.[1] The absence of electron propagation was predicted because of Anderson localization in disordered systems, eventually causing conductive materials to be insulating.[2,3] Since it originates from the interference of coherent waves,[4] Anderson localization can be extended from an electron to other waves, such as electromagnetic waves,[5−11] acoustic waves,[12−14] and matter waves.[15,16] So far, the localization of light has drawn significant attention. Strong localization of light can be realized in periodic[17−19] or quasiperiodic[20−23] dielectric structures, and it is represented by photonic band gaps. On a contrary condition, i.e., in a completely random medium, strong localization of light can be formed due to fully random scattering of light.[24−26] Furthermore, a relatively weak disorder, such as a disorder with short-range correlations, can also lead to a strong localization of light.[27−33] Although experimental demonstration of Anderson localization of electrons remains a challenge of the possibility of bound states in a disordered potential, direct observation of Anderson localization of light has been successfully performed,[8,34−38] stimulating applications in imaging, solar energy,[31] random lasing,[39−42] and optical transition.[43]

On the other hand, surface plasmon polaritons (SPPs) are electromagnetic excitations propagating on the interface between a dielectric and a conductor. Due to the strong field confinement and enhancement effects, SPPs have attracted significant attention.[44] Yet so far, only very limited examples have been shown with near-field approaches in fully random systems.[45,46] Bozhevolnyi et al.[46] have proposed to use channels in strongly scattering nonabsorbing random media for guiding electromagnetic waves, and have successfully demonstrated such a concept with near-field microscopy. The ab initio analyses have theoretically shown that a structural disorder can induce localization of light in 1D and 2D random arrays of coupled metallic nanowires.[47] Very recently, Anderson localization of "spoof" surface plasmons has been successfully observed in terahertz devices.[48] However, due to the intrinsic field damping on metal surfaces at optical frequencies, it is difficult to observe strong localization of SPPs in the visible regime. Yet, on the other hand, since Anderson localization of SPPs associates spatial-disorder-induced light localization with SPP-induced light confinement, it can be applied to achieve stronger field confinement for various applications, such as strong light-matter interactions, surface-enhanced Raman scattering,[49−51] and random lasing on nanoscale.

Here we experimentally demonstrate the realization of strong localization of SPPs at visible regime by controlling the degree of disorder in metal nanogratings. In our experiments, the

Received: December 10, 2017
Revised: February 6, 2018
Published: February 12, 2018

DOI: 10.1021/acs.nanolett.7b05191
Nano Lett. 2018, 18, 1896−1902

short-range correlated disorder of the nanograting induces sufficiently strong interference between multiple scattered SPPs and provides adequate fluctuation distribution of the effective permittivity in the plasmonic system. Consequently, the SPP confinement is enhanced and the SPP propagation is suppressed by increasing the disorder degree in nanogratings. As a result, Anderson localization of SPPs appears at visible regime, which is represented by the exponentially decaying electric fields, the dramatically reduced propagation length of the SPPs, and correspondingly the vanishing autocorrelation function. In this way, we eventually achieve strong localization of SPPs at optical frequencies with an engineered disorder.

The experimental samples are a series of 1D silver (Ag) nanogratings fabricated on SiO_2 substrates, for which we first deposit a silver film of thickness d = 60 nm by magnetron sputtering, followed by etching the gratings with focus-ion beam milling. Two types of silver gratings are fabricated: one is a periodic grating, and the other type consists of aperiodic gratings with different degrees of disorder. The periodic Ag grating (Sample I) has a period p = 250 nm and slit width w = 50 nm, and the total number of slits is N = 50. For the aperiodic gratings, the disorder[52] is introduced by changing the separation of the slits while preserving the slit width w = 50 nm. The disorder degree of the grating can be defined as $\eta = \Delta x/p$, where p is the grating period and Δx is a random deviation of the slit from the position of a periodic grating. In this work, we examine aperiodic silver gratings with disorder degrees from η = 10−60%. This range is divided into 12 disorder degrees. For each disorder degree, more than 15 samples with different slit arrangements have been fabricated. Thus, nearly 200 samples have been investigated. As two typical examples, Figure 1a,b shows the scanning electron microscope (SEM) images of the periodic silver grating (Sample I) and a disordered silver grating with disorder degree η = 40% (Sample II), respectively.

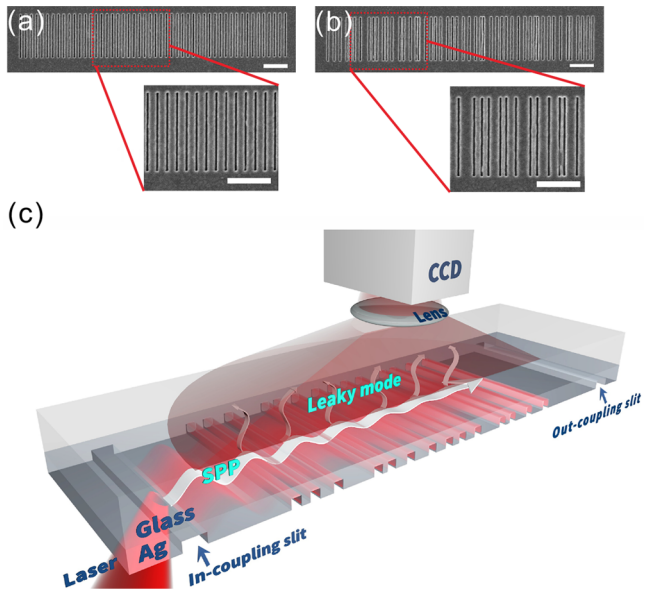

Figure 1. SEM images of (a) the periodic nanograting (Sample I) and (b) a disordered nanograting with disorder degree η = 40% (Sample II). Insets show the magnified details. Each scale bar is 1 μm. The slit width is always w = 50 nm, and the grating period of part a is p = 250 nm. Both gratings consist of 50 slits. Thickness of the silver films is d = 60 nm. (c) Schematic of the experimental setup. The incident laser is coupled into the surface with a single slit, and the SPPs then propagate into the grating. The leaky mode can be captured to trace the propagation of the SPPs.

With the fabricated sample, we measure the in-plane SPP propagation in the nanogratings. When the SPPs transport along the silver nanograting, some of the SPPs can tunnel through the slits, while the others are localized around the slits, as schematically shown in Figure 1c. Thus, we can trace the SPP propagation either by observing the propagating SPPs or recording the localized SPPs. In our experiments, we place the SiO_2 substrate face up and the silver film containing the slits face down (Figure 1c). A supercontinuum laser placed under the sample acts as an excitation source; the wavelength is set at λ = 680 nm, and transverse magnetic (TM) polarization is used. A parallel groove is fabricated in the silver film to couple the free-space incident light to launch the SPPs. The SPPs then propagate on the surface of the silver film. First, we directly trace the propagating SPPs by collecting the signal from the out-coupling slit located at the end of the grating (Figure 1c). As shown in Figure 2, a very bright spot can be observed from the out-coupling slit in the periodic case. However, when the disorder degree increases in the nanogratings, the out-coupled light dramatically decays and eventually disappears. The observations imply that the SPPs can indeed be localized in the disordered grating.

Meanwhile, the localized SPPs can be used to trace the SPP propagation through the nanograting with a leaky mode. When the SPPs reach the silts, leaky modes are excited. It is known that for a leaky mode, the relationship between two propagating constants k_x (along propagation direction) and k_z (perpendicular to propagation direction) can be described[53] as $k_x^2 + k_z^2 = k_{SPP}^2$. Here k_{SPP} is the wave vector of the SPPs at the Ag/air interface, i.e., $k_{SPP} = k_{air}\sqrt{\varepsilon_{air}\varepsilon_{Ag}/(\varepsilon_{air} + \varepsilon_{Ag})}$, where ε_{air} and ε_{Ag} are the permittivity of air and silver, respectively. The SPPs can be often reflected in the nanogratings, and the corresponding Bragg wavelength follows $\lambda \approx 2n_{eff}p$, where n_{eff} is the effective refractive index of nanograting[54,55] and p is the grating periodicity. In our case, the leaky modes transmit through the silver and SiO_2 layers. Finally, these leaky modes of SPPs are collected by a lens (schematically shown in Figure 1c). A charge-coupled device (CCD) camera is applied to image the leaky modes, from which we can directly record the in-plane SPP propagation. Figure 3b shows the recorded images of the leaky modes (λ = 680 nm) of seven typical grating samples together with the SEM micrographs (Figure 3a). Here the first sample is a periodic grating, and the other six samples are disordered gratings with η = 10−60%, respectively. Remarkably, in the periodic grating, SPPs can transmit through the structure over a long distance (>10 μm); however, in the disordered gratings, the propagation lengths dramatically decrease, and the electric fields become localized. As the degree of disorder increases, the propagation length clearly decreases, and the SPPs are more strongly localized.

To verify experimental data, we apply a full-wave finite-difference time-domain (FDTD) method to calculate the propagation of SPPs in different structures including periodic and disordered gratings. The calculated electric-field distributions of the current seven gratings are shown in Figure 3c. We can see that the simulations seem to show a threshold of ~40% for reaching the localization, while the experimental results in Figure 3b show a monotonic decrease of the propagation length for SPP. The deviation between experiments and simulations comes mainly for two reasons. One is that the experimental

DOI: 10.1021/acs.nanolett.7b05191
Nano Lett. 2018, 18, 1896−1902

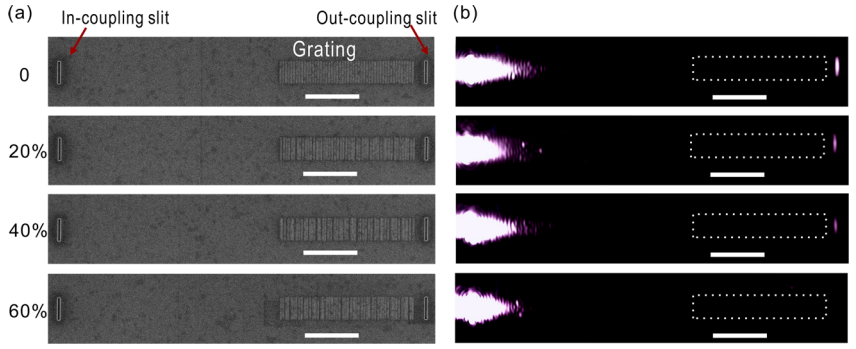

Figure 2. (a) Samples with an out-coupling slit at the end of the grating. Each scale bar is 5 μm. Note that the gratings should be shallow enough in order to observe the signal from the out-coupling slit. (b) CCD recorded images of the samples. In the experiments, we place the SiO_2 substrate face up and the silver film containing the slits face down. The in-coupling slit is fabricated to couple the laser for launching the SPPs. The out-coupling slit is placed at the end of the grating to couple the in-plane SPPs and radiate light to free space.

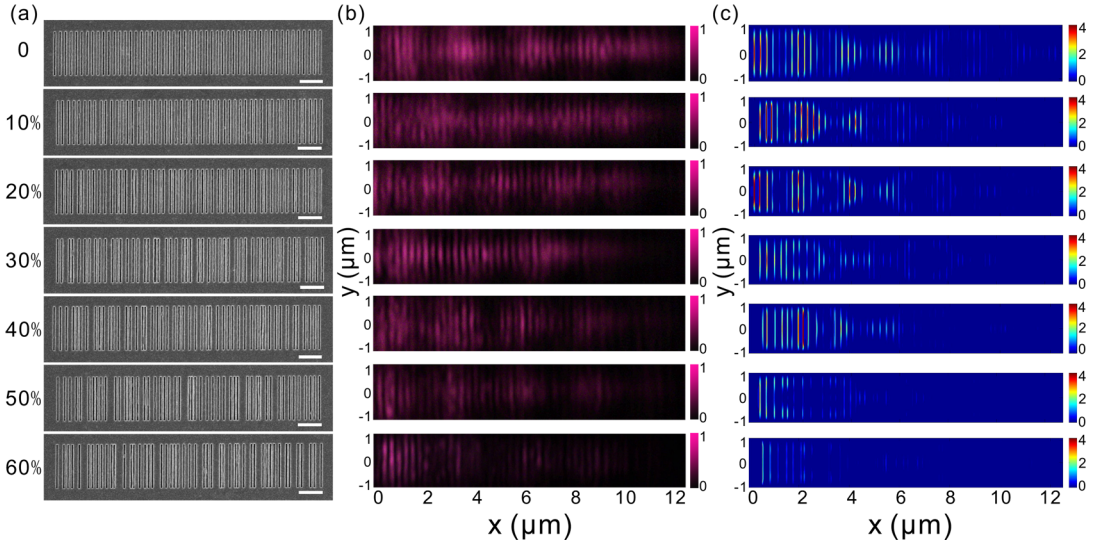

Figure 3. (a) SEM images of a periodic nanograting (η = 0) and six typical disordered nanogratings with disorder degrees from η = 10−60% with increments of 10%. The scale bar is 1 μm. (b) CCD recorded leaky mode images of the corresponding samples at λ = 680 nm, showing that SPPs can be localized in these nanogratings with a correlated disorder. (c) Calculated electric-field intensity distributions, which are consistent with the experimental results in part b.

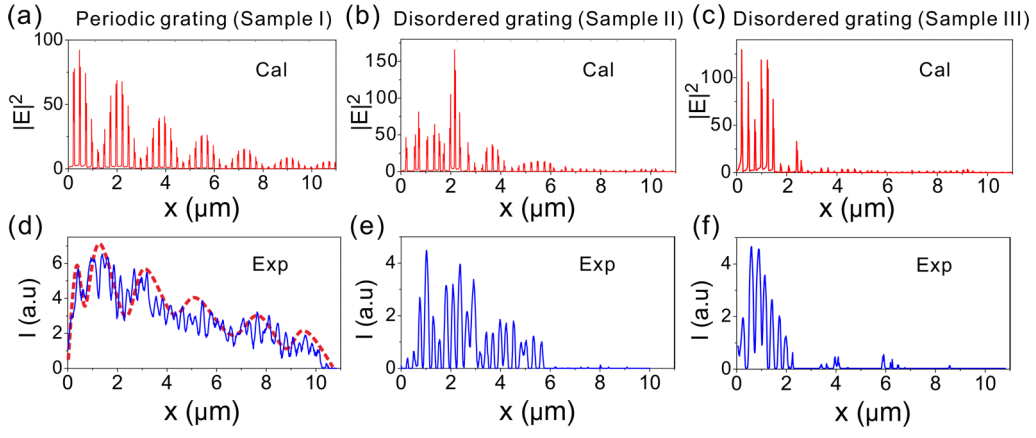

Figure 4. Calculated (a) and measured (d) spatial distributions of the electric-field intensity at λ = 680 nm in the periodic nanograting (Sample I). The dashed line in part d shows the outline of the experimental data. Calculated (b and c) and measured (e and f) distributions of the electric-field intensity in the disordered nanogratings with a different disorder degree (Sample II with η = 40% and Sample III with η = 60%), showing localization of the SPPs in the disordered structure. The consistency between the calculations and measurements also demonstrates the reliability of using the leaky mode to observe the SPPs in experiments.

DOI: 10.1021/acs.nanolett.7b05191
Nano Lett. 2018, 18, 1896−1902

data are collected at far field based on leaky modes, which definitely disperse in the space, whereas the simulated electric distributions are collected at near field. The other reason is that the surface roughness of the samples also affects the experimental results; while in the simulation, the sample surface is supposed to be smooth. However, the calculated distributions are mainly consistent with the experimental results for both periodic and disordered gratings, which confirm that indeed the electric fields can propagate through the periodic grating, but localize in systems with an increasing degree of disorder.

Next, we try to quantitatively study the localization of the SPPs in the silver gratings with different degrees of disorder. To show the localization of SPPs along the propagation direction (x-direction), we integrate the field intensity in the y-direction (perpendicular to the x-direction) so as to obtain the electric-field distribution as a function of x. Figure 4a–f shows the calculated and experimental distributions in the periodic (Sample I), the 40%-disordered (Sample II), and the 60%-disordered (Sample III) structures. In the periodic sample, we can observe the frequent oscillations of the localized SPPs around the slits, and the envelope oscillations from the effective cavity modes in the periodic grating. Clearly, with increasing disorder, the propagation modes previously observed in periodic structures have vanished in the disordered structure, and the SPPs become localized in the disordered structure. Here, we show only two typical disordered examples; yet, in our experiments, we have recorded the propagation of SPPs in 200 samples with different disorder degrees from η = 10–60%.

The samples are divided into 12 disorder degrees, and for each degree, more than 15 samples with different slit arrangements have been examined. At each disorder degree, the confinement of the SPPs is quantified by the inverse participation ratio $P = \int I^2(x)dx \Big/ \left(\int I(x)dx\right)^2$, which has the unit of inverse length. The effective propagation length is $L_{\text{eff}} = \langle P \rangle^{-1}$, where $\langle \cdots \rangle$ stands for averaging over multiple realizations of disorder. Experimentally, I is obtained from the CCD images, while in the calculation, the intensity is represented by $|E|^2$. In Figure 5, the averaged inverse participation ratio and the effective propagation length are presented as a function of the disorder degree in the samples. It follows that, as the disorder degree increases, the inverse participation ratio increases, and the effective propagation length decreases. Both of them converge at larger disorder degrees. In the calculation, we determine the electric-field intensity on the silver surface (near fields), in the experiment; however, we measure the light intensity of the leaky mode, where the distribution of the leaky modes is more extended than the near-field distributions, as illustrated in Figure 3b,c. Consequently, the value of L_{eff} obtained by the calculations are smaller than that from the experiments. Nevertheless, similar tendencies demonstrate that measuring the leaky mode is a reliable way to investigate the surface wave. Thus, both the calculated and experimental results reveal that the localization of the SPPs originates from the disorder in the gratings. Once the degree of disorder reaches approximately 40%, direct observations on the leaky modes show that the electric fields of the SPPs exponentially decay along the propagation direction, and the effective propagation length decreases below 2 μm. Therefore, plasmonic Anderson localization indeed emerges in metallic nanogratings with a correlated disorder.

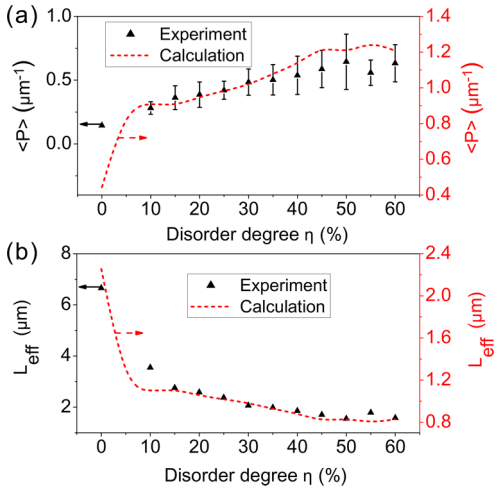

Figure 5. (a) The averaged inverse participation ratio P and (b) the effective propagation length L_{eff} as a function of the disorder degree in disordered nanogratings. Experimental (left black axis) and calculated (right red axis) data are shown. Both P and L_{eff} vary with the disorder degree η and tend to converge at a higher η.

It is worth discussing the origin and mechanisms of the SPP localization in metallic nanogratings with a correlated disorder. Because the gratings we studied are 1D structures, we consider only 1D propagation of SPPs described by

$$\frac{d^2E}{dx^2} + \frac{\omega^2}{c^2 n^2}\varepsilon_{\text{eff}}E = 0 \tag{1}$$

where ω is the circular frequency, c is the speed of light in vacuum, and n is the refractive index in vacuum. Here $\varepsilon_{\text{eff}} = \varepsilon + \Delta\varepsilon$ is the effective permittivity of the entire disordered structure, where ε the effective permittivity of the period is structure and $\Delta\varepsilon$ is the permittivity change due to the short-range correlated disorder. From eq 1, we obtain the electric field as

$$E(x) = E_0 \exp\left(i\frac{\omega}{c}\sqrt{\varepsilon_{\text{eff}}}\cdot x\right) \tag{2}$$

$$\sqrt{\varepsilon_{\text{eff}}} = \sqrt{\varepsilon + \Delta\varepsilon} = \sqrt{\varepsilon}\left[1 + \frac{1}{2}\frac{\Delta\varepsilon}{\varepsilon} - \frac{1}{8}\left(\frac{\Delta\varepsilon}{\varepsilon}\right)^2 + \cdots\right] \tag{3}$$

If we write the in-plane wave vector of the SPPs in the periodic structure as $k_x = \frac{\omega}{c}\sqrt{\varepsilon} \equiv k_1 + ik_2$, the electric field in the 1D correlated-disorder structure can be described as

$$E(x) = E_0 \exp(ik_1 x)\cdot\exp\left(ik_1\frac{\Delta\varepsilon}{2\varepsilon}x\right)\cdot\exp\left[-ik_1\frac{1}{8}\left(\frac{\Delta\varepsilon}{\varepsilon}\right)^2 x\right]\cdots$$
$$\times \exp(-k_2 x)\cdot\exp\left(-k_2\frac{\Delta\varepsilon}{2\varepsilon}x\right)\cdot\exp\left[k_2\frac{1}{8}\left(\frac{\Delta\varepsilon}{\varepsilon}\right)^2 x\right]\cdots \tag{4}$$

Since $\Delta\varepsilon$ depends on the disorder, the electric-field distribution is also affected by the disorder. In fact, the localization effect of the SPPs is influenced by the short-range correlated disorder in two ways. First, it is affected by the inherent attenuation part of the SPPs. As the propagation length of the SPPs increases, the intensity of the electric field decreases. The permittivity fluctuation due to the short-range

DOI: 10.1021/acs.nanolett.7b05191
Nano Lett. 2018, 18, 1896–1902

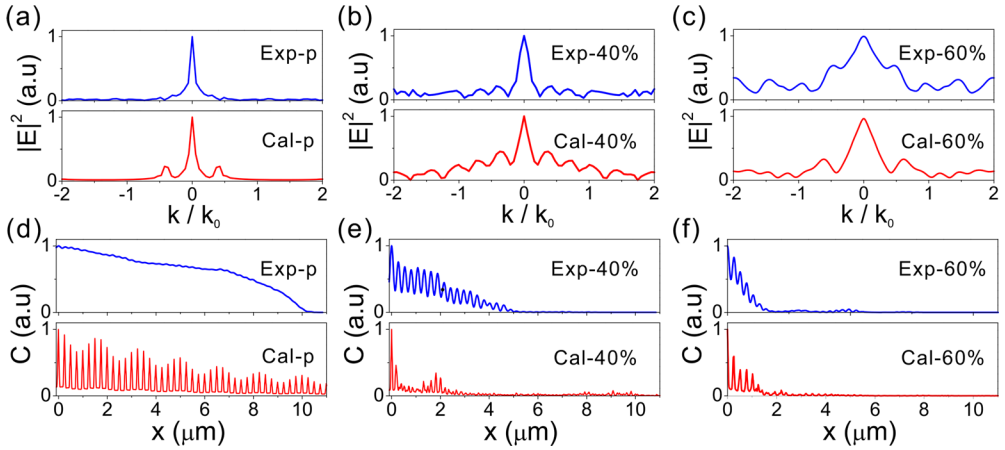

Figure 6. Fourier transform of the experimental and calculated electric-field intensity distributions at λ = 680 nm in (a) the periodic nanograting (η = 0, Sample I) and the disordered nanogratings with (b) η = 40% (Sample II) and (c) η = 60% (Sample III), respectively. The autocorrelation functions of the experimental and calculated data for (d) the periodic nanograting, and the disorder nanograting with (e) η = 40% (Sample II) and (f) η = 60% (Sample III), respectively. Here the autocorrelation disappears in disordered structures because of the coupling between multiple scattered modes.

disorder supplies additional attenuation, indicating that the electric-field intensity will decrease more quickly in disordered structures than in periodic structures. Second, the permittivity fluctuation from the disorder leads to changes in the wave vector in eq 4, and the change can be positive or negative. Therefore, the short-range disorder leads to various SPPs with different wave vectors. The superposition of these multiple SPP waves destroys the propagation modes in otherwise periodic structures. Thus, as the degree of the disorder increases, SPPs are localized, indicating that plasmonic Anderson localization emerges in the grating with correlated disorder. This conclusion has been confirmed by Figures 4 and 5.

We have also analyzed the electric-field distributions as functions of wave vectors in the periodic, the 40%-disordered, and the 60%-disordered structures based on the Fourier transform (FT) method. In Figure 6a–c, the wave vectors have been normalized by k_{SPP}, which is the wave vector of the SPPs at a flat Ag surface without any nanostructures. Comparing with the periodic structure, more wave vectors arise randomly in the disordered structure (Figure 6b,c), in agreement with eq 4. Those multiple modes with various wave vectors are strongly coherent, and their collective effect eventually leads to SPP localization. Moreover, it is known that the autocorrelation function[56] can be utilized to analyze the correlation feature of various disordered structures. In general, there is no autocorrelation in disordered structures. Here, we adopt the autocorrelation function to analyze the electric-field distributions of SPPs in the nanogratings:

$$C(x) = \int f(x)\cdot f^*(\xi + x)d\xi \tag{5}$$

where $f(x)$ is the electric-field intensity. Figure 6d shows that, in the periodic structure, the value of the autocorrelation function remains nonzero over the entire grating. However, in the disordered structures (Figure 6e,f), the autocorrelation function quickly vanishes as x increases. The autocorrelation results together with the FT analyses thus prove that the short-range correlated disorder induces multiple SPPs with various wave vectors, and those SPP waves are strongly scattered, which lead to the disappearance of the autocorrelation and consequently give rise to Anderson localization of the SPPs. In principle, these highly localized SPP modes in such correlated-disorder structures may have many applications. For example, they can be used as resonators to add functionality to the components of the SPPs, to provide the basis for random nanolasing.[31]

In summary, we have demonstrated a controllable realization of strong localization of SPPs at visible regime in disordered metal nanogratings by tuning the short-range correlated disorder. When strong localization of the SPPs occurs at optical frequencies, the electric fields of the SPPs exponentially decay, and the effective SPP propagation length dramatically shrinks. These effects can also be quantitatively described by the autocorrelation among the scattered SPPs that vanishes in sufficiently strong disordered gratings. Although our experiments are carried out on 1D structures, it is anticipated that strong localization of the SPPs can also be realized in 2D and 3D correlated-disorder systems. The underlying mechanism is that the short-range correlated disorder triggers strong interference among scattered SPPs and stimulates field confinement via the permittivity fluctuation, leading to strong localization of the SPPs that can be efficiently tuned by engineering the disorder. Thus, our study enriches the family of Anderson localization and sheds new light on developing disorder engineering in plasmonic systems. We expect that these effects can achieve promising applications in random nanolasing, solar energy, and strong light-matter interactions.

Methods. *Fabrication of Samples.* The experimental samples are a series of 1D silver (Ag) nanogratings fabricated on SiO_2 substrates, for which we first deposit a silver film of thickness d = 60 nm by magnetron sputtering, followed by etching the gratings with focus-ion beam milling (FIB, Helios Nanolab 600i).

Measurement of the SPPs' in-Plane Propagation. In the experiments, we place the SiO_2 substrate face up and the silver film containing the slits face down (Figure 1c). A supercontinuum laser (Fianum, SC400) placed under the sample acts as an excitation source, where the wavelength is set at 680 nm (λ = 680 nm) and transverse magnetic (TM) polarization is used. A parallel groove is fabricated in the silver film to couple the free-space incident light to launch the SPPs. The SPPs then propagate on the surface of the silver film. When the SPPs reach the silts, the leaky modes are excited, and then they

DOI: 10.1021/acs.nanolett.7b05191
Nano Lett. 2018, 18, 1896–1902

transmit through the silver and SiO_2 layers. Finally, these leaky modes of the SPPs are collected by an oil lens. A charge-coupled device (CCD) camera is applied to image the leaky modes.

Numerical Simulation of the SPPs' in-Plane Propagation. Based on the full-wave finite-difference time-domain (FDTD) method, we carry out the numerical simulation on the transportation of the SPPs on the silver nanogratings by using a commercial software package (Lumerical, FDTD_Solutions version 8.0.1). The geometry is modeled as that of the measured samples. Focused Gaussian sources are used in the simulation.

■ ASSOCIATED CONTENT

Supporting Information

The Supporting Information is available free of charge on the ACS Publications website at DOI: 10.1021/acs.nanolett.7b05191.

Experimental and simulated results, schematic diagrams, effective propagation lengths, and inverse participation ratios from the samples with various disorder degrees (PDF)

■ AUTHOR INFORMATION

Corresponding Authors

*E-mail: rwpeng@nju.edu.cn.
*E-mail: xiahuang@aps.anl.gov.
*E-mail: muwang@nju.edu.cn.

ORCID

Ruwen Peng: 0000-0003-0424-2771

Author Contributions

R.P. conceived the idea. W.B.S. fabricated the samples. W.B.S., D.H.X., L.Z.L., K.Z., and J.H. characterized the samples and performed the measurements. W.B.S. performed the calculations. Q.J.W. helped to fabricate the samples. R.H.F. helped to perform the measurements. W.B.S., R.P., M.W., and X.R.H. analyzed and interpreted the data and implications. W.B.S., R.P., X.R.H., and M.W. wrote the Letter. R.P., X. R. H., and M.W. supervised the research.

Notes

The authors declare no competing financial interest.

■ ACKNOWLEDGMENTS

This work was supported by the National Key R&D Program of China (2017YFA0303702), the National Natural Science Foundation of China (11634005, 61475070, 11474157, 11674155, and 11621091), and partially by the "333 project" from the Jiangsu province (BRA2016350). X.R.H. was supported by the U.S. Department of Energy, Office of Science, Office of Basic Energy Sciences, under contract no. DE-AC02-06CH11357.

■ REFERENCES

(1) Anderson, P. W. *Phys. Rev.* **1958**, *109*, 1492−1505.
(2) Lee, P. A.; Ramakrishnan, T. V. *Rev. Mod. Phys.* **1985**, *57*, 287−337. Byczuk, K.; Hofstetter, W.; Yu, U.; Vollhardt, D. *Eur. Phys. J.: Spec. Top.* **2009**, *180*, 135−151.
(3) Pixley, J. H.; Goswami, P.; Sarma, S. D. *Phys. Rev. Lett.* **2015**, *115*, 076601.
(4) Sheng, P. *Introduction to wave scattering, localisation and mesoscopic phenomena*; Springer: Berlin, Germany, 2006.
(5) John, S. *Phys. Rev. Lett.* **1987**, *58*, 2486−2489.
(6) Raedt, H. D.; Lagendijk, A.; Vries, P. D. *Phys. Rev. Lett.* **1989**, *62*, 47−50.
(7) Chabanov, A. A.; Stoytchev, M.; Genack, A. Z. *Nature* **2000**, *404*, 850−853.
(8) Schwartz, T.; Bartal, G.; Fishman, S.; Segev, M. *Nature* **2007**, *446*, 52−55.
(9) Levi, L.; Krivolapov, Y.; Fishman, S.; Segev, M. *Nat. Phys.* **2012**, *8*, 912−917.
(10) Segev, M.; Silberberg, Y.; Christodoulides, D. N. *Nat. Photonics* **2013**, *7*, 197−204.
(11) Riboli, F.; Caselli, N.; Vignolini, S.; Intonti, F.; Vynck, K.; Barthelemy, P.; Gerardino, A.; Balet, L.; Li, L. H.; Fiore, A.; Gurioli, M.; Wiersma, D. S. *Nat. Mater.* **2014**, *13*, 720−725.
(12) He, S. J.; Maynard, J. D. *Phys. Rev. Lett.* **1986**, *57*, 3171−3174.
(13) Smith, D. T.; Lorenson, C. P.; Hallock, R. B.; McCall, K. R.; Guyer, R. A. *Phys. Rev. Lett.* **1988**, *61*, 1286−1289.
(14) Hu, H.; Strybulevych, A.; Page, J. H.; Skipetrov, S. E.; Van Tiggelen, B. A. *Nat. Phys.* **2008**, *4*, 945−948.
(15) Billy, J.; Josse, V.; Zuo, Z. C.; Bernard, A.; Hambrecht, B.; Lugan, P.; Clément, D.; Palencia, L. S.; Bouyer, P.; Aspect, A. *Nature* **2008**, *453*, 891−894.
(16) Roati, G.; D'Errico, C.; Fallani, L.; Fattori, M.; Fort, C.; Zaccanti, M.; Modugno, G.; Modugno, M.; Inguscio, M. *Nature* **2008**, *453*, 895−899.
(17) Notomi, M.; Yamada, K.; Shinya, A.; Takahashi, J.; Takahashi, C.; Yokohama, I. *Phys. Rev. Lett.* **2001**, *87*, 253902.
(18) Akahane, Y.; Asano, T.; Song, B. S.; Noda, S. *Nature* **2003**, *425*, 944−947.
(19) Vlasov, Y. A.; Bo, X. Z.; Sturm, J. C.; Norris, D. J. *Nature* **2001**, *414*, 289−293.
(20) Peng, R. W.; Wang, M.; Hu, A.; Jiang, S. S.; Jin, G. J.; Feng, D. *Phys. Rev. B: Condens. Matter Mater. Phys.* **1998**, *57*, 1544−1550.
(21) Wang, Y. Q.; Hu, X. Y.; Xu, X. S.; Cheng, B. Y.; Zhang, D. Z. *Phys. Rev. B: Condens. Matter Mater. Phys.* **2003**, *68*, 165106.
(22) Maciá, E. *Rep. Prog. Phys.* **2012**, *75*, 036502.
(23) Vardeny, Z. V.; Nahata, A.; Agrawal, A. *Nat. Photonics* **2013**, *7*, 177−187.
(24) Wiersma, D. S.; Bartolini, P.; Lagendijk, A.; Righini, R. *Nature* **1997**, *390*, 671−673.
(25) Van Albada, M. P.; Lagendijk, A. *Phys. Rev. Lett.* **1985**, *55*, 2692−2695.
(26) Leonetti, M.; Karbasi, S.; Mafi, A.; Conti, C. *Phys. Rev. Lett.* **2014**, *112*, 193902.
(27) Kaliteevski, M. A.; Martinez, J. M.; Cassagne, D.; Albert, J. P. *Phys. Rev. B: Condens. Matter Mater. Phys.* **2002**, *66*, 113101.
(28) Peng, R. W.; Liu, Y. M.; Huang, X. Q.; Qiu, F.; Wang, M.; Hu, A.; Jiang, S. S.; Feng, D.; Ouyang, L. Z.; Zou, J. *Phys. Rev. B: Condens. Matter Mater. Phys.* **2004**, *69*, 165109.
(29) Lahini, Y.; Avidan, A.; Pozzi, F.; Sorel, M.; Morandotti, R.; Christodoulides, D. N.; Silberberg, Y. *Phys. Rev. Lett.* **2008**, *100*, 013906.
(30) Patterson, M.; Hughes, S. *Phys. Rev. Lett.* **2009**, *102*, 253903.
(31) Wiersma, D. S. *Nat. Photonics* **2013**, *7*, 188−196.
(32) Conley, G. M.; Burresi, M.; Pratesi, F.; Vynck, K.; Wiersma, D. S. *Phys. Rev. Lett.* **2014**, *112*, 143901.
(33) Mafi, A. *Opt. Lett.* **2015**, *40*, 3603−3606.
(34) Topolancik, J.; Ilic, B.; Vollmer, F. *Phys. Rev. Lett.* **2007**, *99*, 253901.
(35) Lahini, Y.; Pugatch, R.; Pozzi, F.; Sorel, M.; Morandotti, R.; Davidson, N.; Silberberg, Y. *Phys. Rev. Lett.* **2009**, *103*, 013901.
(36) Levi, L.; Rechtsman, M.; Freedman, B.; Schwartz, T.; Manela, O.; Segev, M. *Science* **2011**, *332*, 1541−1544.
(37) Mascheck, M.; Schmidt, S.; Silies, M.; Yatsui, T.; Kitamura, K.; Ohtsu, M.; Leipold, D.; Runge, E.; Lienau, C. *Nat. Photonics* **2012**, *6*, 293−298.
(38) Sperling, T.; Buhrer, W.; Aegerter, C. M.; Maret, G. *Nat. Photonics* **2013**, *7*, 48−52.
(39) Cao, H.; Ling, Y.; Xu, J. Y.; Cao, C. Q. *Phys. Rev. Lett.* **2001**, *86*, 4524−4527.

DOI: 10.1021/acs.nanolett.7b05191
Nano Lett. 2018, 18, 1896−1902

(40) Wiersma, D. S. *Nat. Phys.* **2008**, *4*, 359−367.
(41) Liu, J.; Garcia, P. D.; Ek, S.; Gregersen, N.; Suhr, T.; Schubert, M.; Mørk, J.; Stobbe, S.; Lodahl, P. *Nat. Nanotechnol.* **2014**, *9*, 285−289.
(42) Hsieh, P.; Chung, C.; McMillan, J. F.; Tsai, M.; Lu, M.; Panoiu, N. C.; Wong, C. W. *Nat. Phys.* **2015**, *11*, 268−274.
(43) Maguid, E.; Yannai, M.; Faerman, A.; Yulevich, I.; Kleiner, V.; Hasman, E. *Science* **2017**, *358*, 1411−1415.
(44) Berini, P.; Leon, I. D. *Nat. Photonics* **2012**, *6*, 16−24.
(45) Grésillon, S.; Aigouy, L.; Boccara, A. C.; Rivoal, J. C. *Phys. Rev. Lett.* **1999**, *82*, 4520−4523.
(46) Bozhevolnyi, S. I.; Volkov, V. S.; Leosson, K. *Phys. Rev. Lett.* **2002**, *89*, 186801.
(47) Shi, X. L.; Chen, X. F.; Malomed, B. A.; Panoiu, N. C.; Ye, F. *Phys. Rev. B: Condens. Matter Mater. Phys.* **2014**, *89*, 195428.
(48) Pandey, S.; Gupta, B.; Mujumdar, S.; Nahata, A. *Light: Sci. Appl.* **2016**, *6*, e16232.
(49) Kneipp, K.; Wang, Y.; Kneipp, H.; Perelman, L. T.; Itzkan, I.; Dasari, R. R.; Feld, M. S. *Phys. Rev. Lett.* **1997**, *78*, 1667−1670.
(50) Xu, H. X.; Bjerneld, E. J.; Käll, M.; Börjesson, L. *Phys. Rev. Lett.* **1999**, *83*, 4357−4360.
(51) Huang, Y. Z.; Fang, Y. R.; Zhang, Z. L.; Zhu, L.; Sun, M. T. *Light: Sci. Appl.* **2014**, *3*, e199.
(52) Ren, X. P.; Fan, R. H.; Peng, R. W.; Huang, X. R.; Xu, D. H.; Zhou, Y.; Wang, M. *Phys. Rev. B: Condens. Matter Mater. Phys.* **2015**, *91*, 045111.
(53) Zia, R.; Selker, M. D.; Brongersma, M. L. *Phys. Rev. B: Condens. Matter Mater. Phys.* **2005**, *71*, 165431.
(54) Jetté-Charbonneau, S.; Charbonneau, R.; Lahoud, N.; Mattiussi, G.; Berini, P. *Opt. Express* **2005**, *13*, 4674−4682.
(55) Zhang, X.; Ma, Z.; Luo, R.; Gu, Y.; Meng, C.; Wu, X. Q.; Gong, Q. H.; Tong, L. M. *Nanotechnology* **2012**, *23*, 225202.
(56) Jacobs, D.; Nakanishi, H. *Phys. Rev. A: At., Mol., Opt. Phys.* **1990**, *41*, 706−719.

DOI: 10.1021/acs.nanolett.7b05191
Nano Lett. 2018, 18, 1896−1902